Draft version October 25, 2010
Preprint typeset using LaTeX style emulateapj v. 11/10/09

ASSESSING THE ROLE OF SPIN NOISE IN THE PRECISION TIMING OF MILLISECOND PULSARS

Ryan M. Shannon and James M. Cordes
Astronomy Department, Cornell University, Ithaca, NY 14853
Draft version October 25, 2010

ABSTRACT

We investigate rotational spin noise (referred to as timing noise) in non-accreting pulsars: millisecond pulsars, canonical pulsars, and magnetars. Particular attention is placed on quantifying the strength and non-stationarity of timing noise in millisecond pulsars because the long-term stability of these objects is required to detect nanohertz gravitational radiation. We show that a single scaling law is sufficient to characterize timing noise in millisecond and canonical pulsars while the same scaling law underestimates the levels of timing noise in magnetars. The scaling law, along with a detailed study of the millisecond pulsar B1937+21, leads us to conclude that timing noise is latent in most millisecond pulsars and will be measurable in many objects when better arrival time estimates are obtained over long data spans. The sensitivity of a pulsar timing array to gravitational radiation is strongly affected by any timing noise. We conclude that detection of proposed gravitational wave backgrounds will require the analysis of more objects than previously suggested over data spans that depend on the spectra of both the gravitational wave background and of the timing noise. It is imperative to find additional millisecond pulsars in current and future surveys in order to reduce the effects of timing noise.

Subject headings: gravitational waves — pulsars: general — pulsars: specific (PSR B1937+21) — stars: neutron

1. INTRODUCTION

In most pulsars the residual times of arrival (TOAs) show structure that differs greatly from what is expected from measurement error alone and is typically consistent with having a red power spectrum. This structure is generically referred to as spin noise or timing noise (TN).

Rotational irregularities of the neutron star appear to be the dominant source of TN in most pulsars. Timing noise is thought to arise from either changes in coupling between the neutron star crust and its superfluid core (Jones 1990) or magnetospheric torque fluctuations (Cheng 1987; Kramer et al. 2006; Cordes & Shannon 2008; Lyne et al. 2010). Thus the study of TN provides valuable insight into the structure of the neutron star and its magnetosphere.

The observed strength of timing noise varies by more than eight orders of magnitude over the known non-accreting pulsars, which we subdivide into three classes: the magnetars, with spin frequencies $\nu < 1/6\ \mathrm{s}^{-1}$ and relatively high magnetic fields; the rapidly-spinning and relatively weakly magnetized millisecond pulsars (MSPs), with spin frequencies $\nu > 50\ \mathrm{s}^{-1}$; and the canonical pulsars (CPs) with both spin frequencies and magnetic field strengths between the two other classes. Some magnetars show root mean square (rms) TOA variations of many tens of seconds on time scales of years, whereas the most stable MSPs have not shown evidence of TN at the 200 ns level over decade-long time scales.

Millisecond pulsars, which have stability comparable to the best terrestrial clocks, continue to be intensely studied. Their low levels of TN enable other TOA perturbations to be quantified, such as the relativistic effects in pulsars with massive (white dwarf) companions (Verbiest et al. 2008), recoil from planetary-mass companions (Konacki & Wolszczan 2003), and the presently-undetected stochastic background of gravitational waves (Detweiler 1979; Hellings & Downs 1983; Jenet et al. 2006). Interest in the detection of gravitational waves with pulsars has intensified in recent years due to the improvement in MSP timing precision. This improvement can be attributed to technological advancements in telescope receivers and signal processing equipment (Demorest 2007), improved analysis methods (van Straten 2006), and the discovery of new pulsars that appear to possess intrinsically superior timing stability (Ord et al. 2006).

Long-term timing stability of millisecond pulsars is necessary to detect the small correlated perturbations in the TOAs associated with passage of gravitational waves through the solar system. It has been suggested that if sub-100 ns stability over $5-10$ years can be achieved for a number of millisecond pulsars (currently estimated at $N_{\mathrm{PTA}} = 20-40$) in a pulsar timing array (PTA), a stochastic background of gravitational waves at a cosmologically significant level can be detected (Jenet et al. 2005). Only two MSPs have shown any measurable TN, making characterizing as well as forecasting TN in MSPs difficult. However, the strength and properties of TN will certainly affect the detection of gravitational waves, even if TN is latent in most objects at present.

In this paper we analyze TN throughout the pulsar population and assess the strength of TN in MSPs. In §2 we summarize the phenomenology of TN and show that random walk models and related non stationary processes can be used to model most observed TN. In §3 we suggest two tools for diagnosing TN: one that is appropriate for assessing the long-term stability of MSPs and another that can be used to classify and compare TN throughout the pulsar population. In §4, we derive scal-

ryans@astro.cornell.edu
cordes@astro.cornell.edu

ing relationships for TN in canonical pulsars, millisecond pulsars, and magnetars. We find that millisecond pulsars have TN that is consistent with that observed in canonical pulsars. We further link MSPs to CPs by showing that the behavior of the MSP B1937+21 is similar to that found in the canonical pulsar population. In contrast, magnetars are found to possess TN that exceeds the amount expected from extrapolation from the other populations. In §5 we conclude that TN is present at levels that affect the observation strategies employed in pulsar timing arrays and suggest detecting gravitational radiation requires timing observations of more pulsars than previously estimated. In that section we also discuss techniques for mitigating TN and improving the sensitivity of a PTA to gravitational waves.

2. TIMING NOISE: PHENOMENOLOGY

Timing noise is manifested as structure in the residuals of a fit to pulsar TOAs. A single TOA is determined by comparing a profile formed from averaging a large number of pulses with a template profile. The averaging is conducted to both increase the signal to noise ratio and decrease the effects of jitter associated with intrinsic pulse-to-pulse phase and amplitude variations. The TOAs are then compared to a model that accounts for the propagation of the pulse from the pulsar to the earth and refers the arrival times to the solar system barycenter (Edwards et al. 2006). The fit includes terms accounting for periodic variations associated with the motion of the earth about the solar system barycenter and the reflex motion of the pulsar due to a companion, if the pulsar is in a binary system. The fit also includes secular terms that account for the unknown spin-down of the pulsar, and secular, but frequency-dependent terms that correct for the propagation of the radio pulses through plasma in the interstellar medium. It is essential to fit for the pulsar spin frequency ν and frequency derivative $\dot{\nu}$ because these quantities are intrinsic to the pulsar and cannot be predicted using any other technique. With the exception of a few young pulsars (such as the Crab and Vela pulsars) the values of the higher order frequency derivatives associated with pulsar braking are not measurable on the year to decade observing spans over which pulsars have presently been observed.

The residuals $\mathscr{R}(t)$ of the fit are used to assess the validity of the timing model and identify the presence of unmodeled periodic and secular trends. The rms of the residuals over an observing span of length T, after a second-order polynomial fit is given by

$$\sigma^2_{\mathscr{R},2}(T) = \frac{1}{N_t}\sum_i^{N_t} \mathscr{R}^2(t_i), \quad (1)$$

for an observation comprising N_t samples at times t_i, with $i = 1, N_t$.

The variance $\sigma^2_{\mathscr{R},2}$ can be subdivided into a white component σ^2_W and a red component $\sigma^2_{\rm TN,2}$ that in canonical pulsars is usually dominated by TN:

$$\sigma^2_{\mathscr{R},2}(T) = \sigma^2_{\rm TN,2}(T) + \sigma^2_W. \quad (2)$$

In this discussion *red* is used to label processes which have ensemble average power spectra that have greater power at lower fluctuation frequencies (red spectra) and *white* for processes that have equal levels of power at all fluctuation frequencies (white or flat spectra).

There are a number of TN models that are distinguished by the time evolution of the residuals, or equivalently the shape of the power spectrum of the residuals.

One set of models is based on random walks of the spin properties of the pulsar. We consider random walks in pulse phase ($\rm RW_0$), frequency ($\rm RW_1$), and frequency derivative ($\rm RW_2$) as useful archetypal processes. Because the processes correspond to white noise in ν, $\dot{\nu}$, and $\ddot{\nu}$, they produce rms residuals that scale proportional to $T^{1/2}$, $T^{3/2}$, and $T^{5/2}$, respectively (Boynton et al. 1972), and ensemble average power spectra with spectral indices of -2, -4, and -6, respectively (Harding et al. 1990). For these processes the residuals have non-stationary statistics. For reference, we note that a gravitational wave background from merging massive black holes produces rms residuals that scale proportional to $T^{5/3}$ and a power spectrum with a spectral index of $-13/3$ (Jaffe & Backer 2003).

Band-limited noise (BL) is associated with processes that have low and high frequency cut-offs, in which the rms residuals increase for some time with a slope dependent on the particular spectral shape of the process. After a time associated with the low-frequency cut-off of the band $T_{\rm out} = 1/f_{\rm low}$, the rms timing noise will plateau. An example of a BL process is the perturbation induced by a wide asteroid belt around a pulsar (R. Shannon et al., in preparation).

In many pulsars it appears that multiple types of TN occur at once. However, random walks provide a good basis for modeling non-stationary components of timing noise. Cordes & Downs (1985) and D'Alessandro et al. (1995) conducted detailed analyses of complementary sets of canonical pulsars. While they found that TN in most canonical pulsars cannot be explained by a single random walk process, both suggest that a mixture of random walks in ν and $\dot{\nu}$ and discrete jumps in ϕ, ν, and $\dot{\nu}$ were compatible with the TN.

Alternative models for timing noise include periodic and quasiperiodic processes. These models have gained favor because of recent reports of periodic and quasiperiodic contributions the the residual TOAs for a few pulsars. For example, PSR B1931+24 (Kramer et al. 2006) shows jumps between two states with distinct spin down rates $\dot{\nu}$ at quasiperiodic times. In a study of 366 pulsars, Hobbs et al. (2010) and Lyne et al. (2010) identify a few pulsars ($\approx 2\%$ of their sample) that contain periodic or quasiperiodic components in residual time series and switches between distinct states of $\dot{\nu}$. They also found that the different levels of $\dot{\nu}$ have unique average pulse profiles and they propose that this form of timing noise can be corrected. In a substantial fraction of the identified cases of periodicity or quasiperiodicity, the model included a significant $\ddot{\nu}$ that is attributed to non-stationary timing noise that augments any periodic or quasiperiodic component. We discuss the possibility of mitigating timing noise further in §5.3.

While in some cases, there is clear evidence of a periodic or quasiperiodic contribution to the TOAs, in other cases, realization to realization variation can mimic quasiperiodic behavior. To demonstrate this we simulated residual curves for $\rm RW_0$, $\rm RW_1$, and $\rm RW_2$ random

walks. In the top panel of Figure 1, we show four realizations of quadratic-subtracted residual TOAs for the same RW_1 process. In the plots residual curves show behavior that mimic quasiperiodicity, irregular behavior in which higher order polynomials dominate the TN, and cubic-dominated behavior with both $\ddot{\nu} > 0$ and $\ddot{\nu} < 0$.

We use the number of zero crossings to quantify the morphological variations in single realizations of RW processes. Realizations that have a large number of zero crossings will appear quasiperiodic or irregular. In contrast, realizations that have three zero crossings will appear cubic and match what is expected from ensemble average statistics. In the bottom panel of Figure 1 we show a histogram of the number of zero crossings for each quadratic-subtracted polynomial for 4000 realizations of RW_1, and RW_2 processes. A significant fraction of the realizations of both RW_1 and RW_2 processes show > 3 zero crossings and a few show > 6 zero crossings. The number of zero crossings for residuals of RW_0 random walks is not displayed, because this random walk has a shallow spectrum and thus single realizations show very irregular behavior that typically have > 10 zero crossings.

3. TIMING NOISE: DIAGNOSTICS

Two approaches have been used to characterize the strength of timing noise in radio pulsars. The first uses the total TN after a second order fit $\sigma_{\rm TN,2}$. Cordes & Helfand (1980) define the activity parameter as

$$A = \log\left[\frac{\sigma_{\rm TN,2}(T)}{\sigma_{\rm TN,2}(T)_{\rm Crab}}\right], \quad (3)$$

which measures levels of TN relative to the Crab pulsar and represents a time-independent measure of the strength of the TN, assuming that pulsars show TN with similar time variability to the Crab pulsar.

A second set of methods characterizes timing noise using the frequency second derivative $\ddot{\nu}$ calculated from a cubic fit to the TOAs. Some groups have directly used $\ddot{\nu}$ to assess the strength of the TN (Urama et al. 2006; Chukwude 2007) and correlated it with other pulsar parameters. Arzoumanian et al. (1994) assessed the strength of TN using a parameter

$$\Delta_8 = \log\left(\frac{|\ddot{\nu}|}{6\nu}T_8^3\right), \quad (4)$$

where $\ddot{\nu}$ is measured over an observing span of $T_8 = 10^8$s. While the cubic term will dominate the variance of TN in the ensemble average of any red process with a monotonically decaying spectrum, in a single realization higher order terms may contain a large portion of the TN. Thus statistics based on $\ddot{\nu}$ tend to underestimate the amount of TN in these processes. Additionally, the statistic Δ_8 is model-dependent because $\ddot{\nu}$ on average increases with length of observing span for red noise processes, much like the total rms residuals. Therefore to properly compare values of Δ_8 or $\ddot{\nu}$ in observations of different lengths a model-dependent time scaling needs to be included.

A dimensionless Allan variance-like parameter σ_z is described in Matsakis et al. (1997) that can be used to estimate pulsar stability,

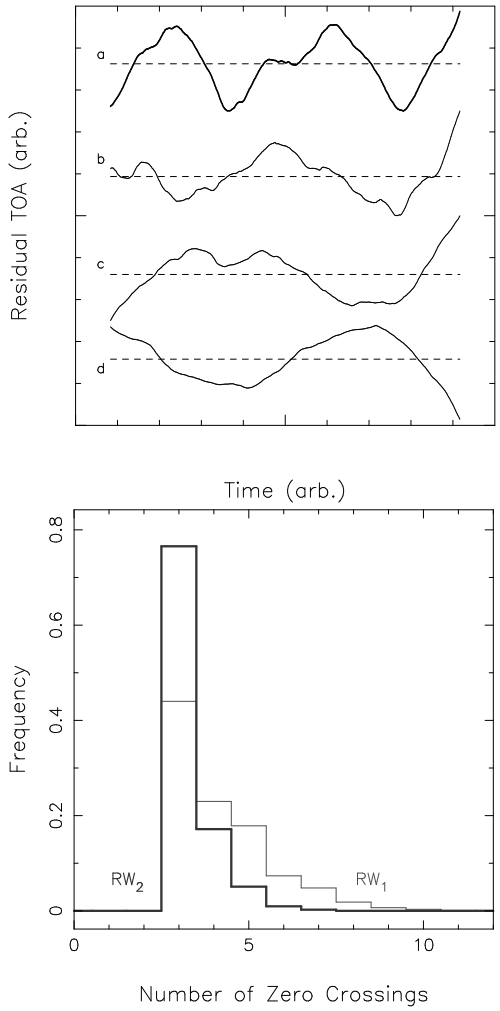

Figure 1. *Upper panel:* Four realizations of RW_1 timing noise. Curve *a* has a large number of zero crossings and behavior that could be misidentified as quasi-periodic in spectral analysis. Curves *b* shows behavior that is irregular. Curves *c* and *d* show behavior in which the cubic term is dominant, with $\ddot{\nu} > 0$ in curve *c* and $\ddot{\nu} < 0$ in curve *d*. *Bottom panel:* Histogram of the number of zero crossings for processes RW_1 (thick lines) and RW_2 (thin lines) after including a quadratic fit. Both processes show realizations where the number of zero crossings is much larger than 3 that mimic quasiperiodicity in spectral analyses. The number of zero crossings for RW_0 is off the scale of the graph.

$$\sigma_z(T) = \frac{1}{2\sqrt{5}}\left[\frac{\sigma_{\ddot{\nu}}(T)}{\nu}\right]T^2, \quad (5)$$

where $\sigma_{\ddot{\nu}}(T)$ is the rms of $\ddot{\nu}$ over observing spans of length T. Because the parameter uses $\ddot{\nu}$ to estimate TN, it also will in general underestimate the total TN.

Previous methods do not provide satisfactory diagnostics for TN. We therefore suggest that the rms timing noise (after a second order fit) is the basis for any proper diagnostic of TN, and propose two closely-related tools for diagnosing TN in pulsars.

To estimate the timing stability of a pulsar we use the post-fit rms TN scaled to ν, $\dot{\nu}$, and time span T,

$$\hat{\sigma}_{\rm TN,2} = C_2\nu^{\alpha}|\dot{\nu}|^{\beta}T^{\gamma}, \quad (6)$$

where the parameters C_2, α, β, and γ are estimated over

the entire pulsar population.

A diagnostic suitable for comparing timing noise across the pulsar population is the relative TN parameter

$$\zeta = \frac{\sigma_{\rm TN,2}(T)}{\hat{\sigma}_{\rm TN,2}(T)} = \frac{\sigma_{\rm TN,2}(T)}{C_2 \nu^{\alpha} |\dot{\nu}|^{\beta} T^{\gamma}}, \quad (7)$$

which is the measured TN $\sigma_{\rm TN,2}$, normalized by the global fit $\hat{\sigma}_{\rm TN,2}$ from equation (6). The relative TN parameter is similar to the activity parameter A, but instead of normalizing to the properties of one pulsar (i.e., the Crab pulsar), the TN is compared to the best fit across all objects. This statistic can be used to identify outlying objects. If a pulsar shows $\zeta \ll 1$ it has smaller levels of TN than expected. If a pulsar shows $\zeta \gg 1$, it produces larger levels of TN than expected. We note that because this parameter depends on the modeled timing noise it depends on the observations included in the fit. The parameter values will change when more objects are included in the fit, or objects are included over longer observing spans. As a result ζ will change when additional observation of TN are included. If the new observations have statistically similar behavior as the present observations of TN, the fit will not change in a significant way. If the additional objects have different behavior (for example, if timing noise became stationary over very large T), the revised values of ζ will better identify the outlying objects.

4. TIMING NOISE ACROSS NEUTRON STAR POPULATIONS

In this section, we show how rotational TN varies across the canonical pulsar, millisecond pulsar and magnetar populations. Previous analyses of TN have focused on canonical pulsars and fit for only a limited number of parameters using the statistical tools described in the previous section. Instead we will use $\hat{\sigma}_{\rm TN,2}$ and ζ, which are defined in equations (6) and (7), respectively.

For our analysis we compiled observations of TN from many sources in the literature. In Appendix A we present the observing campaigns that we use and describe our methods for calculating $\sigma_{\rm TN,2}$. Our analysis includes $N_t = 1213$ time series, from approximately 450 distinct pulsars, which include $N_D = 591$ detections of TN and $N_{\rm UL} = 622$ upper limits. Our analysis excludes young objects that have measured frequency second derivatives $\ddot{\nu}$ that are attributed to pulsar braking. Plots displaying the rms timing noise $\sigma_{\rm TN,2}$ versus ν and $\dot{\nu}$ are displayed in Figure 2.

4.1. *Maximum Likelihood Analysis*

We use a maximum likelihood approach following Dewey & Cordes (1989) to find the best fit parameters for equation (6) in logarithmic space

$$\ln(\hat{\sigma}_{\rm TN,2}) = \ln C_2 + \alpha \ln(\nu) + \beta \ln|\dot{\nu}_{-15}| + \gamma \ln(T_{\rm yr}), \quad (8)$$

with $\sigma_{\rm TN,2}$ expressed in μs, ν expressed in $\rm s^{-1}$, $\dot{\nu}_{-15}$ expressed in 10^{-15} $\rm s^{-2}$, and $T_{\rm yr}$ expressed in years.

A fifth parameter δ is incorporated in the analysis to account for the large scatter in the strength of the timing noise. This scatter is associated with both realization to realization variation and non-modeled parameters that are assumed to be independent of ν and $\dot{\nu}$, such as neutron star mass and other physical elements of TN.

We assume that $\sigma_{\rm TN,2}$ is log-normally distributed; therefore the probability density function (PDF) of measuring rms residuals $\sigma_{\rm TN,2,i}$ is

$$f_{\sigma_{\rm TN}}(\sigma_{\rm TN,2,i}) = \frac{1}{\sqrt{2\pi\delta^2}} \exp\left[-\left(\frac{\ln(\hat{\sigma}_{\rm TN,2,i}/\sigma_{\rm TN,2,i})^2}{2\delta^2}\right)\right], \quad (9)$$

where $\hat{\sigma}_{\rm TN,2,i} = \hat{\sigma}_{\rm TN,2,i}(C_2, \alpha, \beta, \gamma, \delta)$ is the modeled red noise component. We define the probability P_i as the product of the PDF and the measurement error

$$P_i = f_{\sigma_{\rm TN}}(\sigma_{\rm TN,i}) \Delta(\ln \sigma_{\rm TN,i}) = f_{\sigma_{\rm TN}}(\sigma_{\rm TN,i}) \frac{\Delta\sigma_{\rm TN,i}}{\sigma_{\rm TN,i}}, \quad (10)$$

which assumes that the measurement error is small relative to δ, a situation that is confirmed below.

We also incorporate upper limits from many observations using the probability

$$P_{{\rm UL},i} = 1 - \frac{1}{2}{\rm erfc}\left[\frac{\ln(\hat{\sigma}_{{\rm TN},i}/\sigma_{{\rm TN},i})}{\delta\sqrt{2}}\right], \quad (11)$$

where erfc is the complementary error function. The total probability for N_D detections of timing noise and $N_{\rm UL}$ upper limits is then

$$P(C_2, \alpha, \beta, \gamma, \delta) = \prod_i^{N_D} P_i \prod_j^{N_{\rm UL}} P_{{\rm UL},j}. \quad (12)$$

For each population, the probability space was examined using a series of grid searches. An initial search was conducted with a coarse grid and a wide range of values in each parameter to identify the best-fit location and determine if multiple values of any of the parameters were allowed. Refined grid searches were conducted with much narrower ranges in values with fine gridding to calculate parameter estimation error and covariance.

4.2. *Canonical Pulsars*

A fit restricted to only the canonical pulsars yields well determined values of the parameters in equation (6). We find significant correlation of the strength of timing noise with ν, $\dot{\nu}$, and T. The estimated parameter values and their respective $\pm 2\sigma$ (95%) confidence intervals are presented in Table 1. The scaling of timing noise with observing span ($\gamma = 1.9 \pm 0.2$) is found to be intermediate to scalings expected from $\rm RW_1$ and $\rm RW_2$, for which we would expect $\gamma = 3/2$, and $\gamma = 5/2$, respectively.

Realization to realization variation associated with a stochastic process provides insufficient scatter account for the spread in timing noise that is characterized by the fit parameter $\delta = 1.6 \pm 0.1$. We simulated a large number of realizations of random walks $\rm RW_0$, $\rm RW_1$, and $\rm RW_2$ and determined that realization to realization variation will induce a scatter in each process of $\delta = 0.23$, 0.46, and 0.60, respectively. We conclude that the inferred value of δ includes additional contributions from the actual TN processes that are not captured by single idealized random walk models.

These findings generally agree with previous studies of timing noise in canonical pulsars that have concluded both that TN typically shows non-stationary behavior characterized by a red power spectrum and have established correlations between timing noise and other spin

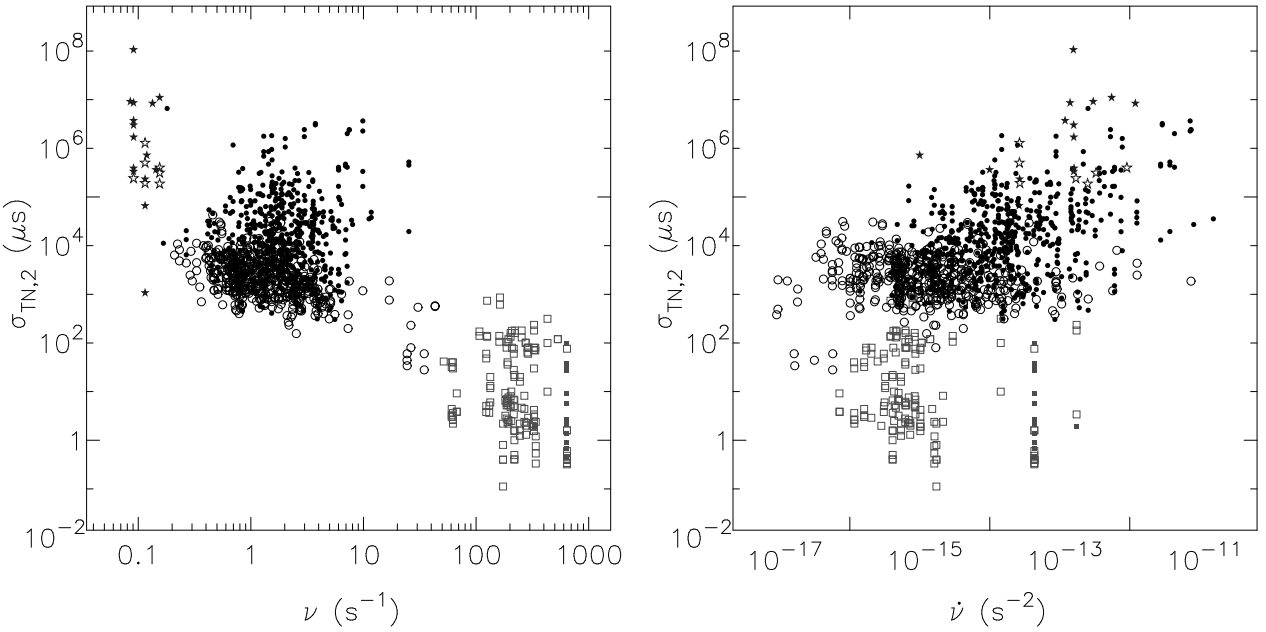

Figure 2. Scatter plots showing the correlation between measured rms timing noise $\sigma_{\rm TN,2}$ with spin frequency ν (left panel) and frequency derivative, $\dot{\nu}$ (right panel). Filled symbols represent detections of timing noise, and open symbols represent 2σ upper limits. Magnetars ($\nu < 1/6$ s^{-1}) are identified by stars, canonical pulsars (50 s^{-1} $< \nu <$ 1/6 s^{-1}) are identified by circles, and millisecond pulsars ($\nu > 20$ s^{-1}) are identified by squares. The observations encompass a wide range of observing spans 0.1 yr $< T <$ 30 yr.

parameters. Cordes & Helfand (1980) found a correlation between the activity parameter A and period derivative $\dot{P} = -\dot{\nu}/\nu^2$ in 50 pulsars. Dewey & Cordes (1989) found a correlation between this activity parameter and P and $\dot{P}$ in observations of 40 canonical pulsars.

The scaling law models the timing noise over the entire range of observing spans and we find no evidence for band-limited timing noise. In Figure 3 we display the relative TN parameter ζ versus observing span. If timing noise was band-limited over current observing spans, the amount of timing noise would plateau, and at large T, the fit would be poor and $\zeta \ll 1$. In addition we found consistency between fits to CP observations with $T <$ 10 yr and $T >$ 10 yr.

Analysis of a large on-going timing campaign of 366 pulsars at the Jodrell Bank Observatory with observing spans of 10 to 36 years is presented in Hobbs et al. (2010). They calculated a scaling relation between σ_z(10 yr) and ν and $\dot{\nu}$

$$\hat{\sigma}_z(10\ {\rm yr}) = 10^{-11.5}\nu^{-0.4}|\dot{\nu}_{-15}|^{0.8}, \qquad (13)$$

where ν is measured in s^{-1} and $\dot{\nu}_{-15} = 10^{-15}$ s^{-2}. Our scaling relationship $\sigma_{\rm TN,2} \propto \nu^{-0.9\pm0.2}|\dot{\nu}|^{1.0\pm0.05}$ is inconsistent with this. In their analysis, σ_z includes contributions from additive white noise. If we conduct our analysis with $\sigma_{\mathscr{R},2}$ (i.e., include the white noise) instead of only to the red component $\sigma_{\rm TN,2}$, we find a more consistent scaling relationship of $\sigma_{\mathscr{R},2} \propto \nu^{-0.7\pm0.1}|\dot{\nu}|^{0.76\pm0.02}$.

4.3. *Millisecond Pulsars*

Only two MSPs have shown significant levels of timing noise: PSR B1937+21 (discussed in detail below), and PSR B1821−24. (Verbiest et al. 2009). The model for canonical pulsars over-predicts the level of timing noise observed in PSRs B1937+21 and B1821−24, as displayed in Figure 4. For both of these objects, the observed levels of TN are below the levels expected from the CP-only fit by a factor of one to two times δ.

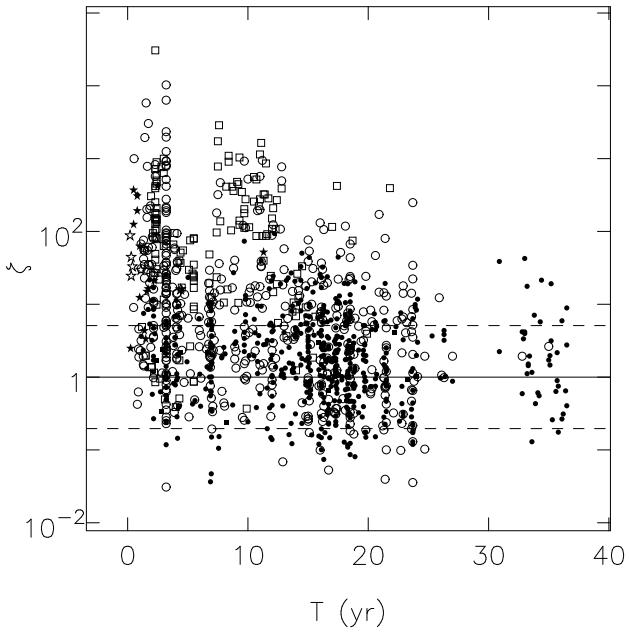

Figure 3. Scatter plot showing the timing noise parameter ζ versus observing span T. We have used the timing noise model of the joint CP+MSP fit to calculate ζ. There is no evidence for a change in timing noise characteristics over longer observing spans. Filled symbols represent detections of timing noise, and open symbols represent 2σ upper limits. Magnetars ($\nu < 1/6$ s^{-1}) are identified by stars, canonical pulsars (50 s^{-1} $< \nu <$ 1/6 s^{-1}) are identified by circles, and millisecond pulsars ($\nu > 20$ s^{-1}) are identified by squares. The solid lines indicates $\zeta = 1$. The dashed lines are the $\pm1\sigma$ variation of ζ, as inferred from value of δ inferred from the joint CP+MSP fit.

The best fit to the MSP population, listed in Table 1, has larger fitting uncertainties because the few observations of TN and constraining upper limits are restricted to smaller ranges in ν, $\dot{\nu}$, and T. The fit is dominated by the many observations of timing noise in PSR B1937+21. For a few MSPs, observations provide restrictive upper limits, but for many the expected levels of timing noise are not constraining at the levels predicted by the CP-only fit.

We also conducted a joint fit of the MSP and CP populations. In Figure 4 (right panel) we plot the observed levels of TN versus the levels predicted from the joint fit. Visual inspection suggests that this fit provides a good model of the timing noise in the MSP population because the levels of timing noise observed are within the $\pm 1\delta$ band and the upper limits exceed levels predicted by the model.

The quality of fit is quantified by comparing observed and predicted levels of timing noise using a χ^2 statistic

$$\hat{\chi}^2 = \sum_i^{N_D} \frac{(\ln \sigma_{\rm TN,2,}{}_i - \ln \hat{\sigma}_{\rm TN,2,}{}_i)^2}{\hat{\delta}^2}, \qquad (14)$$

where only the N_D observations of detected timing noise are included and upper limits are excluded. If a model provides a good fit to the data, $\hat{\chi}^2$ follows a χ^2 distribution. For a fit to any population, the number of degrees of freedom is $N_{\rm DOF} = N_D - 5$ if the population included in the fit (because 5 parameters are included in the fit), and $N_{\rm DOF} = N_D$ if the population was not included in the fit. In Table 2, we list the values of $\hat{\chi}^2$ and corresponding probabilities P that each fit models the individual populations. This analysis confirms that the joint CP+MSP fit is a good model for both the CP and MSP populations.

The similarity of timing noise in MSPs to that in canonical pulsars is strengthened by examining the timing residuals of PSR B1937+21 in greater detail. In terms of statistical precision, PSR B1937+21 is the best MSP in which to study timing noise because it shows the largest levels of TN of any MSP.

In order to assess the strength and type of timing noise in PSR B1937+21, we investigate how $\sigma_{\rm TN,2}$ scales with observing span by combining the results of many timing programs presented in Appendix A. In Figure 5, the rms residual timing noise is plotted versus observing span length for the various campaigns. In this figure we also show model curves for random walks $\rm RW_0$, $\rm RW_1$, and $\rm RW_2$ scaled to an ensemble-average rms of 2 μs over an 8 year observing span, combined in quadrature with a 0.15 μs white noise component, which matches the levels of noise in the short time span observations displayed in Figure 5. Over short time spans, the residuals are dominated by white noise associated with instrumental sensitivity, pulse averaging effects, and diffractive interstellar scintillation (Cordes et al. 1990).

Inspection of this plot shows that the scaling of $\sigma_{\rm TN,2}$ with T is intermediate to $\rm RW_1$ and $\rm RW_2$ and therefore the scaling of TN with time is consistent with the observed scaling in the CP population ($\sigma_{\rm TN} \propto T^{2\pm0.2}$). This scaling is inconsistent with $\rm RW_1$ or $\rm RW_2$ random walks. We note however that the power law scaling is altered if the amplitude of the RW steps have a power-law distribution (for further discussion see Appendix C of Cordes & Downs 1985). The level of TN does not plateau over large T so we conclude that the timing noise shows no sign of being band-limited on the current observation time scales.

Observational bias has lead to detection of TN in only two MSPs. The expected levels of timing noise in the other MSPs are below current observing sensitivity. Timing noise is observed in PSR B1937+21 because it has a considerably larger $\dot{\nu}$ than other intensely studied MSPs.

4.4. *Magnetars*

The probabilities that the models fit the observed TN in the magnetar population are displayed in Table 2. We find that the magnetar-only model provides a good fit to the observations (not surprisingly) but all other models under-predict the timing noise in the magnetar population. We conclude that magnetars show timing noise levels in excess of those found in the other populations of neutron stars.

4.5. *Discussion: Timing Noise in Pulsar Populations*

There are physical reasons to expect timing noise in MSPs and CPs to be consistent and follow a combined power law. Magnetic fields almost certainly play a role in generating timing noise. If surface or magnetospheric magnetic fields play the dominant role (likely the case in the case of a magnetospheric origin of timing noise, and plausibly the case if TN in associated with crust-core interactions), then timing noise would depend on pulsar spin parameters. Differences in the relationship between magnetic field strengths and the spin parameters ν and $\dot{\nu}$ between the populations would cause a break-down in the scaling relations. For example, if timing noise is associated solely with the neutron star core there may be a breakdown in the scaling relationship because both CPs and MSPs may well have similar internal magnetic field strengths despite different spin characteristics.

Ultra-strong magnetic fields may cause the excess timing noise observed in magnetars. Unlike canonical pulsars and millisecond pulsars, magnetar radiation appears to be driven by the decay of magnetic fields, with some theories suggesting that the radiation is associated with crust cracking (Hurley et al. 2005) that may be enhanced compared to CPs. This cracking could drive rotational irregularities that contribute to the observed excess in timing noise.

Many radio pulsars have been discovered that have ν and $\dot{\nu}$ approaching those of the magnetars. Additional timing observations of high magnetic field radio pulsars are needed to properly assess the difference between radio pulsars and magnetars.

5. IMPLICATIONS FOR GRAVITATIONAL WAVE DETECTION

The presence of timing noise will significantly affect the sensitivity of a pulsar timing array to gravitational radiation. At present, most MSPs show residuals consistent with white noise. Based on the scaling laws derived in §4, we predict that TN will be identified in many objects when they are monitored over longer time spans or observed with higher precision.

In Table 3, we list the MSPs that at present show the best timing stability. We show the expected rms timing noise over 2 yr, 5 yr, and 10 yr observing spans, based on

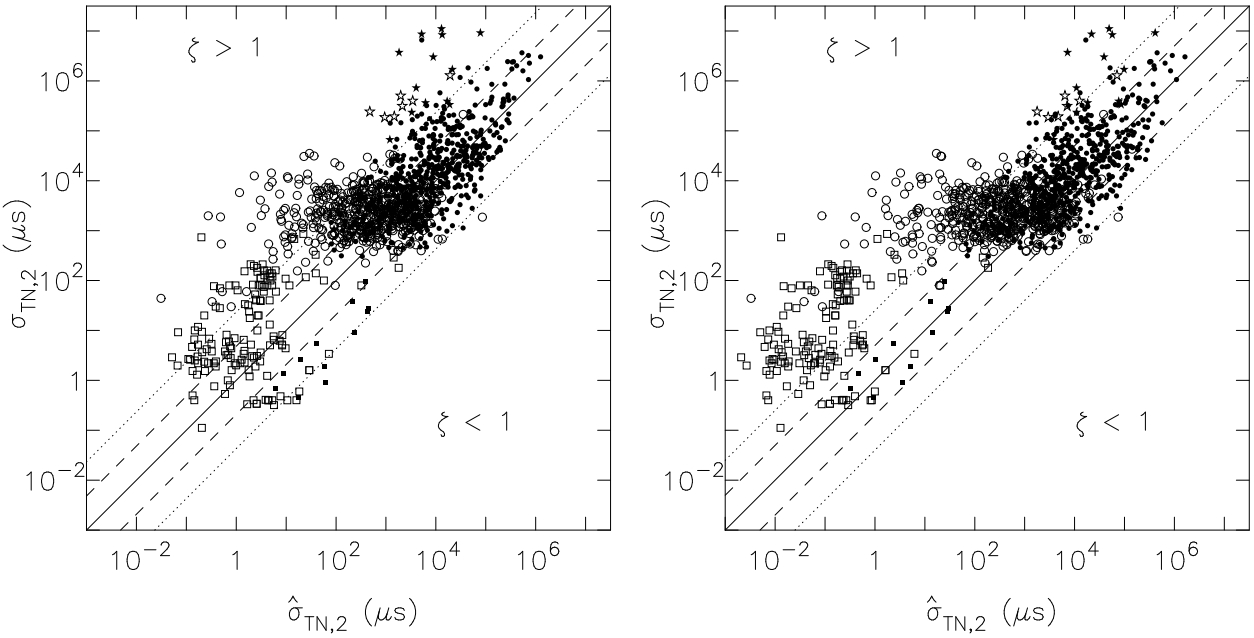

Figure 4. Correlation between predicted rms TN $\hat{\sigma}_{\rm TN,2}$ and measured rms TN $\sigma_{\rm TN,2}$ for the CP-only model (left panel) and the joint CP+MSP model (right panel). Filled symbols represent detections of timing noise, and open symbols represent 2σ upper limits. Magnetars ($\nu < 1/6$ s^{-1}) are identified by stars, canonical pulsars (50 s$^{-1} < \nu < 1/6$ s^{-1}) are identified by circles, and millisecond pulsars (MSPs) are identified by squares. Points above this line are observations that have levels of timing noise greater than expected ($\zeta > 1$). Points below this line are observations that have levels of TN less than expected by the model ($\zeta < 1$). The dashed lines show the expected width as estimated by the parameter $\hat{\delta}$, corresponding the $\pm1\sigma$ (67%) width. The dotted lines show $\pm2\sigma$ (95%) width. The CP-only model overestimates the strength of the timing noise in the MSPs, and both fits underestimate the level of timing noise in the magnetars.

Table 1
Best Fit Parameters

Fit	$\ln(C_2)$	α	β	γ	δ	$N_D(N_{\rm UL})$
CP	2.0 ± 0.4	-0.9 ± 0.2	1.00 ± 0.05	1.9 ± 0.2	1.6 ± 0.1	563 (470)
MSP	-20 ± 20	1 ± 2	2 ± 1	2.4 ± 0.6	1.2 ± 0.5	12 (147)
CP+MSP	1.6 ± 0.4	-1.4 ± 0.1	1.1 ± 0.1	2.0 ± 0.2	1.6 ± 0.1	575 (617)
MAG	3 ± 7	-1 ± 3	1.5 ± 0.6	3 ± 1	2.1 ± 0.7	15 (7)
CP+MAG	2.4 ± 0.5	-1.4 ± 0.2	1.13 ± 0.07	1.7 ± 0.2	1.7 ± 0.2	578 (477)
ALL	2.2 ± 0.4	-1.5 ± 0.1	1.2 ± 0.1	1.8 ± 0.1	1.7 ± 0.1	590 (624)

Note. — Best fit parameters and $\pm2\sigma$ confidence limits for different populations of pulsars. N_D is the number of time series with detected timing noise used in the fit. $N_{\rm UL}$ is the number of time series with upper limits of timing noise used in the fit.

the scaling relationships discussed in §4. We also show the $\pm1\sigma$ variation that would be expected based on the observed spread of timing noise, and measured limits on the amount of TN over 10 yr observing spans. For these pulsars TN is likely present at the 10 ns to 100 ns level and will therefore affect the detection of other TOA perturbations with amplitudes at these levels, such as a gravitational wave background. In addition, we show predicted and measured levels of timing noise for PSR B1937+21. The large levels of timing noise imply this object will not contribute to the sensitivity of a PTA to GWs.

In the following we examine in detail the effect of the presence of timing noise on the properties of the PTA.

5.1. *Timing Noise & PTA Sensitivity*

To estimate the level of timing stability required to detect GWs, we calculate the GW detection signal to noise ratio (SNR) using a particular detection scheme. We note the resulting conclusions are general and are relevant to all detection methods, including methods that are implemented using either frequentist or Bayesian approaches (Jenet et al. 2005; van Haasteren et al. 2009).

5.1.1. *Best Case: Gravitational Waves and Timing Noise Only*

In order to assess the best possible case, we first consider TOAs that contain *only* perturbations associated with gravitational waves and timing noise. For each pulsar k at observation epoch i, the time of arrival perturbation (before any fit) s_{ki} is altered by the correlated component of the GWB passing through the solar neighborhood e_{ki}, the uncorrelated component of the GWB outside of the solar neighborhood p_{ki}, and uncorrelated TN r_{ki}:

$$s_{ki} = e_{ki} + p_{ki} + r_{ki}. \quad (15)$$

Table 2
Fit Comparisons

		Model Fit											
		CP		MSP		MAG		CP+MSP		CP+MAG		ALL	
Family	N_D	χ^2	P	χ^2	P	χ^2	P	χ^2	P	χ^2	P	χ^2	P
CP	563	532	0.8	$10^{5.2}$	(10^{-20})	1996	(10^{-20})	538	0.72	477	0.99	493	0.98
MSP	12	37	$10^{-3.6}$	14	0.05	38	$10^{-3.8}$	3.8	0.8	3.7	0.99	7.0	0.4
MAG	15	176	(10^{-20})	$10^{4.1}$	(10^{-20})	10	0.4	98	(10^{-10})	63	$10^{-7.1}$	54	$10^{-7.5}$

Note. — Goodness of fit estimates for the canonical pulsars (CP), millisecond pulsars (MSP), and the magnetars (MAG) for models of sub-populations. For the model fits the N_D detected time series were used to calculate a χ^2 statistic to assess the goodness of fit for the subgroups of the pulsar population. Using this statistic, we calculated the probability P that a fit modeled the observed levels of timing noise. Probabilities in parentheses are upper limits.

Table 3
Expected Levels Timing Noise for PTA Pulsars

			$T = 2$ yr			$T = 5$ yr			$T = 10$ yr			
Object	ν (s^{-1})	$\dot{\nu}$ ($10^{-15}s^{-2}$)	$\hat{\sigma}_{\rm TN}$ (ns)	$\hat{\sigma}_{{\rm TN},L}$ (ns)	$\hat{\sigma}_{{\rm TN},U}$ (ns)	$\hat{\sigma}_{\rm TN}$ (ns)	$\hat{\sigma}_{{\rm TN},L}$ (ns)	$\hat{\sigma}_{{\rm TN},U}$ (ns)	$\hat{\sigma}_{\rm TN}$ (ns)	$\hat{\sigma}_{{\rm TN},L}$ (ns)	$\hat{\sigma}_{{\rm TN},U}$ (ns)	$\sigma_{\rm TN,meas}$ (ns)
J0437−4715	174	-1.73	35	7	180	210	41	1100	830	160	4300	< 200
J1713+0747	219	-0.41	5	1	26	31	6	160	120	23	630	< 200
J1744−1134	245	-0.54	6	1	31	36	7	190	140	27	730	< 620
J1909−3744	339	-1.62	13	2	68	79	15	410	310	60	1600	< 170
B1937+21	623	-43.30	230	44	1200	1400	270	7200	5500	1100		1500

Note. — Estimated strength of timing noise for selected PTA pulsars and PSR B1937+21 over 2 yr, 5 yr, and 10 yr observing spans based on the best-fit model to the canonical pulsars and the millisecond pulsars (as defined in Table 1). For each pulsar we list the spin frequency ν and spin frequency derivative $\dot{\nu}$. For each observing span we show the expected values $\hat{\sigma}_{\rm TN}$ and the 1σ upper and lower limits: $\hat{\sigma}_{{\rm TN},L}$ and $\hat{\sigma}_{{\rm TN},U}$, respectively. The limits are formally the quadrature sum of the parameter that quantifies the scatter of the distribution $\hat{\delta}$ and the estimation error associated with the model, but are dominated by $\hat{\delta}$. We also present the measured timing noise $\sigma_{\rm TN,meas}$ (or upper limits) over ≈ 10 yr observing span.

The perturbations e and p have the same rms strength. We define the SNR in the time series to be the ratio of the rms amplitudes (after a second order fit) of the correlated portion of the signal (i.e., e_{ki}) to the the uncorrelated portion of the signal ($p_{ki} + r_{ki}$). Thus in the residuals from a single pulsar the SNR is at most unity and is smaller if TN is present.

We now consider one approach to GW detection that involves forming a coherent sum (R. Shannon & J. Cordes, in preparation) of the residuals for $N_{\rm PTA}$ pulsars, which increases the SNR. The best case configuration is when all the pulsars are located in a small patch of the sky, but at different distances away from the observer. In this case e_{ki} is completely correlated between pulsars and p_{ki} and e_{ki} are uncorrelated. As a result, e_{ki} is amplified relative to p_{ki} and r_{ki} by a factor $\sqrt{N_{\rm PTA}}$. The combined SNR in a single data block of span T of observations from $N_{\rm PTA}$ pulsars is

$$\left(\frac{S}{N}\right)_{T,1} = \sqrt{\frac{N_{\rm PTA}\sigma^2_{{\rm GW},2}(T)}{\sigma^2_{{\rm TN},2}(T) + \sigma^2_{{\rm GW},2}(T)}}, \qquad (16)$$

where the rms strengths of the GWB and the TN are characterized by $\sigma_{{\rm GW},2}(T)$ and $\sigma_{{\rm TN},2}(T)$, respectively.

A test statistic based on the coherent sum has an SNR of

$$\left(\frac{S}{N}\right)_{{\rm TS},M} = \sqrt{\frac{MN_{\rm PTA}}{1 + \sigma^2_{{\rm TN},2}(T_M)/\sigma^2_{{\rm GW},2}(T_M)}}, \quad (17)$$

where we have assumed the data set can be subdivided and M independent estimates of the TS can be calculated (for example by using data blocks of length $T_M = T/M$), resulting in an enhancement of the SNR by a factor of $\sqrt{M}$. We note that there are alternative ways to subdivide the time series. Jenet et al. (2006) decompose the residuals using a set of orthonormal polynomials and calculate a TS using each polynomial, while Verbiest et al. (2009) conduct an analysis in the Fourier transform domain. In all cases the optimal value of M is limited by other sources of noise (like white noise), which we discuss further in §5.1.2.

The scaling relationship of equation (17) is used to establish the properties of a PTA sufficient to detect the GWB. To detect the gravitational wave background with a strength $\sigma_{{\rm GW},2}(T)$ with ${\rm SNR}_{{\rm TS},M} > S_{\rm min}$ requires that the TN in an individual pulsar satisfy

$$\sigma_{{\rm TN},2}(T_M) < \sigma_{{\rm GW},2}(T_M)\sqrt{\frac{MN_{\rm PTA}}{S^2_{\rm min}} - 1}. \qquad (18)$$

The number of pulsars required to detect a GWB of strength $\sigma_{{\rm GW},2}(T)$ with an SNR greater than $S_{\rm min}$ with TN at a level $\sigma_{{\rm TN},2}(T)$ is

$$N_{\rm PTA} > \frac{S^2_{\rm min}}{M}\left[1 + \left(\frac{\sigma_{{\rm TN},2}(T_M)}{\sigma_{{\rm GW},2}(T_M)}\right)^2\right]. \qquad (19)$$

Here we make two preliminary estimates of the requirements for GW detection using equations (18) and (19).

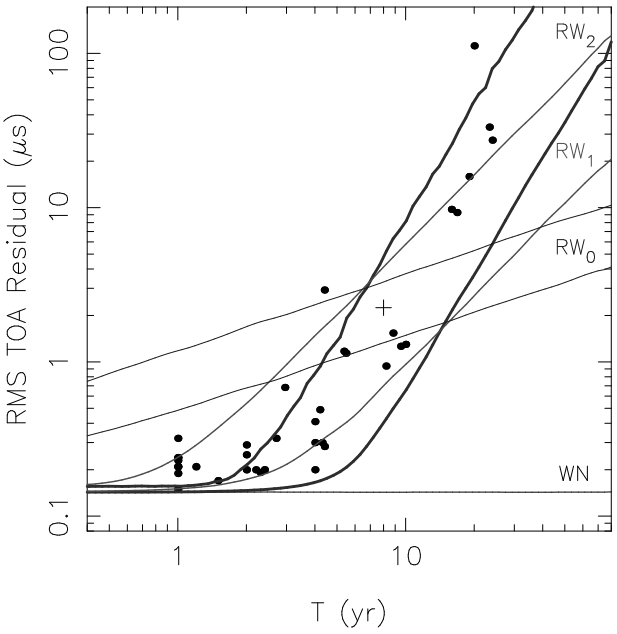

Figure 5. Plot of the rms residuals $\sigma_{\mathscr{R},2} = \sqrt{\sigma_{\rm TN,2}^2 + \sigma_W^2}$ versus observing span T for PSR B1937+21 and simulated random walks. The large scatter in the observations at $T = 1$ yr is associated with variable levels of white noise across timing programs. The expected variation for random walks in phase ϕ ($\rm RW_0$, thinnest lines), frequency ν ($\rm RW_1$, medium thickness lines), and frequency derivative $\dot{\nu}$ ($\rm RW_2$, thickest lines) are also displayed. The 95% confidence limits (based on simulations of a large number of realizations) are shown for each process. The strength of the random walks are normalized to $\sigma_{\rm TN,2} = 2$ μs at $T = 8$ yr, which is indicated by the cross on the plot. To each curve, white noise with rms strength of $\sigma_W = 0.15$ μs is added. This level is denoted by the horizontal line marked WN.

In §5.2 we give a more detailed assessment that uses the model of TN in the pulsar population presented in §4.

As a first example, we estimate pulsar stability requirements to detect the expected stochastic background of merging massive black hole (MBH) binaries. Stochastic GWBs are typically characterized by their expected strain response $h_c(f)$ and not $\sigma_{\rm GW,2}$. In Appendix C we show how to calculate $\sigma_{\rm GW,2}$ from $h_c(f)$. The MBH background is presently considered the strongest plausible GWB, and is expected to induce a strain response of $h_c(f) = A_0(f/1\ {\rm yr}^{-1})^{-2/3}$, where the value of A_0 is estimated to be between 10^{-16} and 10^{-15} (Jaffe & Backer 2003; Sesana & Vecchio 2010). Over a $T = 5$ yr observing span, the MBH GWB will contribute $\sigma_{\rm GW,2} = 19$ ns $(A_0/10^{-15})$ to the times of arrival, as indicated in Table 4, which presents results for this section and for §5.2. To achieve a signal to noise ratio in the detection statistic of $S_{\rm min} = 5$ for a PTA comprising $N_{\rm PTA} = 40$ pulsars using $M = 1$ observation blocks, timing noise must be limited to $\sigma_{\rm TN,2}(T = 5\ {\rm yr}) < (\sqrt{3/5})\sigma_{\rm GW,2}(T = 5\ {\rm yr}) \approx 15$ ns.

We can also estimate the number of pulsars required to detect a GWB if TN levels are equal to the amplitude $\sigma_{\rm TN,2} \approx 20$ ns over 5 years exhibited by the pulsars in Table 3. A PTA comprising $N_{\rm PTA} = 70$ pulsars would yield an SNR of $S_{\rm min} = 5$, assuming $M = 1$, and a GWB with the same properties as in the previous example. However, a number of MSPs are expected to have TN at levels below the scaling law and therefore the required number of pulsars may be somewhat lower, which is described in §5.2

5.1.2. *Effect of White Noise on the Number of Independent Sub-blocks*

In general, the number of subdivisions M that maximizes the SNR of the TS depends on the amplitude of other noise contributions to the residuals, in particular white noise, which is guaranteed to be present in pulsar timing observations. We define a time scale T_M over which the expected GW signal exceeds the white noise levels $\sigma_{W,\rm TS}$ in the coherent time series by the same threshold as the TN, i.e., $\sigma_{\rm GW,2}(T_M) = S_{\rm min}\sigma_{W,\rm TS}(T_M)$. For a total observing span of length T there are $M \approx T/T_{\rm M}$ independent data blocks if $T > T_M$; if not, there is $M = 1$ data block.

The random noise in the TS associated with the WN is given by

$$\sigma_{W,\rm TS}(T) = \frac{\sigma_n}{\sqrt{N_{\rm PTA}N_{\rm obs}(T)}}, \tag{20}$$

where σ_n is the level of white noise in a single observation and $N_{\rm obs}(T) = R_{\rm obs}T$ is the number of observation epochs in the interval of length T, and is characterized by an observation rate $R_{\rm obs}$ (or equivalently an observing cadence of $R_{\rm obs}^{-1}$). For a background with $\sigma_{\rm GW,2}(T) = \sigma_g T^{5/3}$, the minimum time is

$$T_M = \left(\frac{\sigma_n}{\sigma_g}\frac{S_{\rm min}}{\sqrt{N_{\rm PTA}R_{\rm obs}}}\right)^{6/13}. \tag{21}$$

For an array of 40 pulsars, with $N_{\rm obs}(T) = 10\ T_{\rm yr}$ (i.e., 10 observations per year), $\sigma_n = 100$ ns rms error per residual, and a GWB with strain spectrum $h_c(f) = 10^{-15}(f/1\ {\rm yr}^{-1})^{-2/3}$, the minimum block size is $T_{\rm min} \approx 2$ yr for $N_{\rm PTA} = 40$ to 100. The minimum block length $T_{\rm min}$ is approximately the same for both values of $N_{\rm PTA}$ because of the weak dependence of M on $N_{\rm PTA}$, $M \propto N_{\rm PTA}^{3/13}$, for the assumed GWB background.

5.2. *The Fraction of MSPs Suitable for PTAs*

Using the stability requirements defined in equation (18), the fraction of MSPs suitable for inclusion in a PTA, $\mathscr{F}_{\rm MSP}$, can be evaluated. This fraction is equivalent to the probability that a pulsar within the population has rms timing noise less than some threshold amount σ_t over an observing span of length T. Based on our TN model, this probability is

$$P(\ln\sigma < \ln\sigma_t|T) = \int_{-\infty}^{\ln\sigma_t} d\ln\sigma \int d\boldsymbol{M}\rho_{\boldsymbol{M}}(\boldsymbol{M}) \times \int d\nu d\dot{\nu}\rho_{\nu,\dot{\nu}}(\nu,\dot{\nu})\rho_{\ln\sigma}(\ln\sigma|\boldsymbol{M},\nu,\dot{\nu},T), \tag{22}$$

where $\rho_{\boldsymbol{M}}(\boldsymbol{M})$ is the PDF of the parameter distribution, $\rho_{\nu,\dot{\nu}}$ is the PDF of the pulsar distribution in ν and $\dot{\nu}$, and $\rho_{\ln\sigma}$ is the PDF of the level of timing noise, given the model parameters.

In Appendix B, we present methods for evaluating equation (22). The sensitivities of PTAs comprising $N_p = 40$ and 100 pulsars with a variety of observing

Table 4
Timing Noise Constraints on MSPs Suitable for a PTA

		$N_{\rm PTA} = 40$			$N_{\rm PTA} = 100$		
T (yr)	$\sigma_{\rm GW,2}$ (ns)	M	$\sigma_{{\rm TN},2,t}$ (ns)	$\mathscr{F}_{\rm MSP}$ (%)	M	$\sigma_{{\rm TN},2,t}$ (ns)	$\mathscr{F}_{\rm MSP}$ (%)
2	4	1	3	30 ± 7	1	7	46 ± 8
5	19	1	14	25 ± 6	1	32	40 ± 7
10	59	2	28	37 ± 7	3	31	56 ± 7
20	187	5	34	50 ± 7	6	45	64 ± 7
5	19	2	9	41 ± 7	2	15	53 ± 7
5	19	4	4	55 ± 8	4	7	65 ± 7

Note. — Fraction of pulsars suitable for inclusion in a PTA, $\mathscr{F}_{\rm MSP}$, for arrays comprising $N_{\rm PTA} = 40$ and 100 pulsars, over observing spans ranging from $T = 2$ yr to $T = 20$ yr. We have assumed a background with characteristic strain spectrum of $h_c(f) = 10^{-15}(f/1\ {\rm yr}^{-1})^{-2/3}$. We have also assumed a detection signal to noise ratio of $S_{\rm min} = 5$, using equation (18), with M independent data blocks,as described in the main text. Also listed are the quadratic-corrected rms contribution of the gravitational wave background $\sigma_{\rm GW,2}(T)$ for the total observing span T and the threshold TN level $\sigma_{{\rm TN},2,t}(T_M)$ for the sub-block length $T_M = T/M$.

spans T are investigated with the same conditions as in §5.1. We have modeled timing noise $\sigma_{\rm TN,2}$ using the joint CP and MSP model as presented in Table 1 and equation (6).

In Table 4 we show the fraction of pulsars suitable for inclusion in these PTAs. The fraction of suitable pulsars is smaller at $T = 5$ yr than $T = 2$ yr because the level of expected timing noise has increased relative to the GW signal but the number of sub-blocks M has not changed. To produce a PTA comprising $N_{\rm PTA}$ pulsars requires the investigation of a total sample of MSPs, $N_{\rm MSP} = N_{\rm PTA}/\mathscr{F}_{\rm MSP}$ pulsars. To calculate M we have again assumed that the pulsars are observed 10 times per year with an rms precision on a single TOA of 100 ns. For a PTA comprising 40 to 100 high quality MSPs and data spans of 5 to 10 years, our analysis indicates that a total MSP sample that is two to three times larger than $N_{\rm PTA}$ needs to be investigated in order to identify high quality objects.

5.3. *Mitigating Timing Noise*

It has been previously noted that applying a low-pass spectral filter to the residual TOA time series can improve the signal-to-noise ratio in a PTA (Jenet et al. 2005). The presence and diversity of red noise in the MSPs necessitates filtering that is tailored to the properties of each individual pulsar. Schematic power spectra for $\rm RW_0$, $\rm RW_1$, and $\rm RW_2$ random walks and the gravitational wave background are displayed in Figure 6. For systems in which $\rm RW_2$ is the dominant form of TN high-pass filtering (i.e, removing the lowest frequency components of the signal) can be used to mitigate the contribution of TN to the TOAs. It is not possible to develop a filter that mitigates $\rm RW_1$ timing noise without also removing the gravitational wave signal because they have very similar spectral shapes.

There is evidence that pulse profile information can be used to correct residual time series. Lyne et al. (2010) identify a link between changes in pulse shape (probably connected to mode changing) and changes in $\dot{\nu}$, and demonstrate that some timing noise can be corrected by identifying the time of the mode changes and the estimated values of $\dot{\nu}$. Even if all TN is associated with mode changing it is necessary to observe with a short cadence to accurately determine the time at which the change occurred. Lyne et al. (2010) argue that daily observations would be necessary to adequately mitigate this mode changing timing noise in their objects. If objects are not observed with a sufficiently short cadence, the uncertainty in the time of mode change introduces residual timing noise in the corrected time series with an amplitude proportional to the uncorrected level of timing noise. As noted in §3, in half of the cases presented in Lyne et al. (2010), the correlation was found after a fit for $\ddot{\nu}$ that removes non-stationary TN could not be corrected in their data.

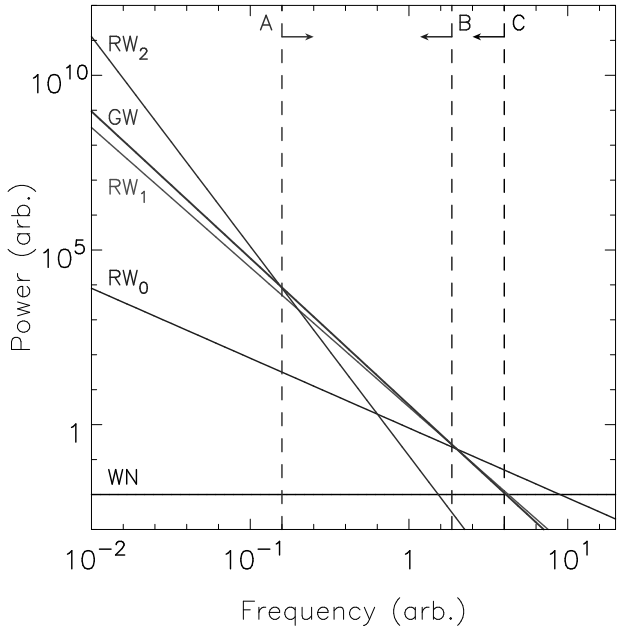

Figure 6. Schematic power spectra for stochastic processes that contribute to pulsar timing residuals. The dashed lines indicate fluctuation frequencies at which the TN exceeds the GWB for various processes and the arrows associated with these lines identify region in which the GWB signal is accessible. Vertical dashed line A identifies the region in which the spin frequency noise ($\rm RW_2$) exceeds the gravitational wave background. Vertical dashed line B identifies the region in which phase noise ($\rm RW_0$) exceeds the gravitational wave background. Vertical dashed line C identifies the region in which white noise (WN) exceeds the gravitational wave background.

5.4. *Future Prospects*

A large number of pulsars need to be studied because timing noise will limit the utility of many objects and MSP timing stability cannot be fully constrained with spin parameters ν and $\dot{\nu}$. As a result, if $N_{\rm PTA}$ pulsars are required for a significant detection of the GWB, a much larger number of pulsars ($N_{\rm MSP} = N_{\rm PTA}/\mathscr{F}_{\rm MSP}$, as outlined in §5.2) need to be discovered and characterized. To constrain the timing stability it is necessary to conduct timing observations with sufficient precision to detect the presence of TN at the threshold level, as set by equation (18). For realistic PTA configurations and a reasonable detection SNR, the required stability level will be at most a factor of a few greater than the anticipated strength of the gravitational wave background.

An object is suitable for inclusion into the PTA if timing noise is not detected at this level.

Pulsar timing arrays can be expanded by both incorporating presently known objects with good intrinsic stability that are currently excluded due to low flux and discovering new MSPs with suitable timing stability.

Additional MSPs suitable for incorporation into a PTA are continually being discovered, with ongoing surveys with the Arecibo, Green Bank, Effelsberg, Parkes Telescopes; targeted searches for radio pulsar companions to *Fermi* gamma-ray point sources; and in the near future with the LOFAR Array (van Leeuwen & Stappers 2010). While occasionally bright MSPs have been discovered (Jacoby et al. 2003), selection effects generally bias new discoveries toward fainter pulsars, and thus suitable objects require longer observations with more sensitive telescopes to mitigate white radiometer noise.

The requirements for finding and timing ultra faint MSPs highlight the need to use high-gain telescopes such as the Arecibo telescope and the proposed Square Kilometre Array (SKA). The SKA is estimated to find up to $\approx$ 6000 MSPs (Smits et al. 2009). If we conservatively estimate that 10% of the MSPs are suitable, there will be $\approx$ 600 objects available for inclusion in a PTA. The very best of these could comprise a PTA sufficient to *detect* the GWB while a much larger PTA could be used to study in detail the GWB and detect and examine individual GW sources. Large interferometers such as the SKA will be particularly important for improving throughput of timing campaigns because they can be divided into sub-arrays that can observe multiple objects simultaneously.

6. CONCLUSIONS

We have developed scaling relationships for timing noise in millisecond pulsars, canonical pulsars, and magnetars. We find that timing noise in MSPs is consistent with that observed in canonical pulsars. The timing behavior of the millisecond pulsar B1937+21 supports universality of TN in CPs and MSPs. Latent timing noise is predicted to be present in other MSPs with similar properties (but smaller) magnitudes to that in the CPs and PSR B1937+21, in accord with their smaller spin down rates. This timing noise may be measurable in many pulsars when either longer data sets or higher precision arrival times are obtained. Timing noise in magnetars is greater than that expected from extrapolation from the canonical pulsars.

We thank George Hobbs for providing a preprint of Hobbs et al. (2010) in advance of publication and the referee for comments that improved the clarity of the text. This work made use of NASA's ADS System and the ATNF Pulsar Catalogue (Manchester et al. 2005). This work was supported by the NSF through grant AST-0807151 and by NAIC, which is operated by Cornell University under a cooperative agreement with the NSF.

APPENDIX

A. REDUCTION PROCEDURE & TIMING CAMPAIGNS USED

We have synthesized the results of many timing observations to construct the scaling relationships for timing noise (TN) in canonical pulsars (CPs), millisecond pulsars (MSPs), and magnetars (MAGs), as described in §4; and to conduct the case study of the MSP B1937+21 (as described in §4.3). In Table 5 we summarize the timing campaigns used in the analyses, the average length of data span contained in the campaign, and the number and type of objects analyzed.

In the following sections we outline the procedure used to properly combine the results from all of the campaigns. In §A.1 we describe how the root mean square (rms) timing noise $\sigma_{\rm TN,2}$ is calculated from other TN diagnostics. In §A.2 we justify the threshold used for detecting the presence of red noise in timing data. In §A.3, we justify the exclusion of some timing observations from this study. In §A.4, we describe the observations used that form the basis of our study of PSR B1937+21.

A.1. *Calculating* $\sigma_{\rm TN,2}$

We use the rms timing noise after a second order polynomial fit $\sigma_{\rm TN,2}(T)$ as the primary observable property of TN, as justified in §3.

In Table 5, for each reference we identify the type of observations reported. While some timing campaigns report $\sigma_{\rm TN,2}$ (coded TN in Table 5), others report different but related measurements of TN. There are two notable conversions that are occasionally needed. Some campaigns report only the total rms residuals and the white noise level, and the red timing noise must be extracted from these quantities. For other campaigns, the timing noise is modeled in a functional form.

Calculating $\sigma_{\rm TN,2}$ from the total timing noise and the white noise (Code TW *in Table 5):* Many timing campaigns report the total rms residuals and the levels of white noise in the observations. In this case, the amount of timing noise is the quadrature difference between the rms residuals $\sigma_{\mathscr{R},2}$ and the white noise in the time series:

$$\sigma^2_{\rm TN,2} = \sigma^2_{\mathscr{R},2} - \sigma^2_W. \tag{A1}$$

In these observations the the level of white noise σ_W reported comes from one of two sources: either the rms of residuals after the TN has been analytically modeled; or an estimate from the white noise in a single TOA.

Including modeled timing noise, (Codes S, STW, or H in Table 5): In some cases the fit includes terms $\mathcal{M}_{\rm TN}(t)$ that model the timing noise. The model is typically a series of polynomials or sinusoids. It is typically included to provide an estimate of $\ddot{\nu}$ (in which case $\mathcal{M}(t) = \ddot{\nu}(t-T_e)^3/6$, where T_e is the epoch at which the spin properties are defined)

or to improve the determination of modeled parameters of interest such as astrometric terms. In these cases $\sigma_{\rm TN,2}$ is approximated as the quadrature sum of the rms of $\mathcal{M}_{\rm TN}(t)$ and the TN contained in the post-fit residuals:

$$\sigma^2_{\rm TN,2} = \sigma^2_{\rm TN,\mathcal{M}}(T) + \frac{1}{T}\int_{t_0}^{t_1} \mathcal{M}^2_{\rm TN}(t)dt, \tag{A2}$$

where t_0 and $t_1 = t_0 + T$ are the starting and ending epochs of the observations.

For observations labeled *S*, polynomials have been used to model the timing noise. For observations labeled *H*, harmonically related sinusoids have been used to model the timing noise. For observations labeled *STW*, a fit including $\ddot{\nu}$ was completed that partially whitens the residuals. In addition to $\ddot{\nu}$, the total rms timing noise $\sigma_{\rm TOT,\mathcal{M}}$ and the whitened rms timing noise σ_W were reported. In this case, the rms timing noise is $\sigma^2_{\rm TN,\mathcal{M}}(T) = \sigma^2_{\rm TOT,\mathcal{M}} - \sigma^2_W$.

A.2. *The Detection Threshold for* $\sigma_{\rm TN,2}$

To determine if timing noise is detected in a time series, we conservatively require that the rms timing noise exceed twice the white noise floor (i.e., $\sigma_{\rm TN,2} > 2\sigma_W$), because we suspect that in many timing programs the residuals were not examined at sufficient detail to rule out TN below this level. If the measured TN in a time series does not meet the threshold we declare the time series to be an upper limit with a value of $2\sigma_W$. This is much larger than the formal detection threshold, $\sigma_{\rm TN,2} > \sigma_W/\sqrt{N_{\rm DOF}}$, where $N_{\rm DOF}$ is the number of degrees of freedom in the residual TOAs.

A.3. *Excluded Observations*

We excluded observations of globular cluster pulsars which show acceleration (and significant $\ddot{\nu}$) associated with these dense environments. We have also excluded some additional reports of timing noise from this analysis:

PSR J1012+5307. Lange et al. (2001) report a non-zero $\ddot{\nu}$ that they attribute to TN. However a more recent analysis by Lazaridis et al. (2009) that includes the previous data shows no evidence for $\ddot{\nu} \neq 0$. We therefore omit the measurement of Lange et al. (2001).

PSR J1713+0747. Splaver (2004) report a non-zero $\ddot{\nu}$ that they attribute to TN. However, a more recent analysis by Verbiest et al. (2009) shows no evidence for $\ddot{\nu} \neq 0$. We therefore exclude the measurement of Splaver (2004).

PSR B1937+21. We have also excluded a measurement of TN for PSR B1937+21 from this analysis, which is discussed in the next section.

A.4. *PSR B1937+21*

The observations used for the analysis of the scaling of the rms TN for PSR B1937+21 (discussed in §4.3) are presented in Table 6. We report the observing span of the observations the rms residuals $\sigma_{\mathscr{R},2}$, and, when available, the number of TOAs used in the analysis. In order to increase the number of independent observations at short observing spans, the publicly available residual TOAs from Kaspi et al. (1994) were subdivided into shorter observing spans of 1, 2, and 4 years. We note that many of the observations contain contemporaneous or common observations, and therefore many of the data points are not formally independent.

All the campaigns included have been corrected for dispersion measure (DM) variations, determined by measuring the arrival time difference contemporaneously in two frequency bands. The DM correction is more accurate in recent campaigns because of improved observation procedures. In early campaigns, the measurements at two frequencies were performed many days apart and changes in interstellar propagation over those times likely increase TOA uncertainty. In more recent campaigns, two-frequency observations often occur consecutively during the same observing session or simultaneously with dual-frequency receivers.

We have excluded the 12.5 yr measurements of timing noise in PSR B1937+21 reported in Verbiest et al. (2009) because the time series contained a long gap between observations with two different instruments. An arbitrary time offset between the two instruments (i.e., a jump) was included the fit. This jump removes a significant amount of TN from the residual time series.

B. ESTIMATING THE FRACTION OF SUITABLE PULSARS

In this section, we describe the methods for calculating the fraction of pulsars suitable for inclusion in the pulsar timing array, $\mathscr{F}_{\rm MSP}$. The fraction of pulsars that show TN below a threshold RMS $\sigma_{{\rm TN},t}$ is equivalent to the probability of finding a pulsar within the population with those properties,

$$P(\ln\sigma < \ln\sigma_t|T) = \int_{-\infty}^{\ln\sigma_t} d\ln\sigma \int d\boldsymbol{M}\rho_{\boldsymbol{M}}(\boldsymbol{M}) \int d\nu d\dot{\nu}\rho_{\nu,\dot{\nu}}(\nu,\dot{\nu})\rho_{\ln\sigma}(\ln\sigma|\boldsymbol{M},\nu,\dot{\nu},T), \tag{B1}$$

where $\rho_{\boldsymbol{M}}$ is the probability density for observing fit parameters, where $\boldsymbol{M} = (C_1, \alpha, \beta, \gamma, \delta)$, as in equation (8); $\rho_{\nu,\dot{\nu}}$ is the probability density for the pulsar spin distribution; and $\rho_{\ln\sigma}$ is the PDF for observing a value of TN, assuming fixed values for the fit parameters.

We will assume that the level of TN σ is log-normally distributed about the expected value:

$$\rho_{\ln\sigma}(\ln\sigma|C_1,\alpha,\beta,\gamma,\delta,\nu,\dot{\nu},T) = \frac{1}{\sqrt{2\pi\delta^2}}\exp\left[-\frac{(\ln\sigma/\hat{\sigma})^2}{2\delta^2}\right]. \tag{B2}$$

This is consistent with the analysis of §4, and the large observed spread in TN for pulsars with similar spin parameters ν and $\dot{\nu}$.

To model the $\rho_{\nu,\dot{\nu}}$, we will use the observed distribution of MSPs:

$$\rho_{\nu,\dot{\nu}}(\nu,\dot{\nu}) = \frac{1}{N_p}\sum_{p}^{N_p}\delta(\nu-\nu_p)\delta(\dot{\nu}-\dot{\nu}_p). \tag{B3}$$

For the analysis presented here, we use the 64 non-globular cluster MSPs listed in the ATNF pulsar catalogue (Manchester et al. 2005).

The parameter space PDF $\rho_{\boldsymbol{M}}$ is modeled using estimates of the best fit values and the fitting covariance matrix $\boldsymbol{C}$

$$\rho_{\boldsymbol{M}}(\boldsymbol{M}|\ln C_1,\alpha,\beta,\gamma,\delta_T) = \frac{1}{\sqrt{(2\pi)^5\det(\boldsymbol{C}^{-1})}}\exp\left[(\boldsymbol{M}-\hat{\boldsymbol{M}})^T\boldsymbol{C}^{-1}(\boldsymbol{M}-\hat{\boldsymbol{M}})\right], \tag{B4}$$

where $M = (\ln C_1,\alpha,\beta,\gamma,\delta)^T$ and $\hat{M}$ is a vector containing the best fit parameters to the joint CP+MSP fit. For ease of computation, the PDF was approximated using a large number $N_s = 10^5$ of parameter values drawn from equation (B4):

$$\rho_{\boldsymbol{M}} = \frac{1}{N_s}\sum_{s}^{N_s}\delta(\ln C_1-\ln C_{1,s})\delta(\alpha-\alpha_s)\delta(\beta-\beta_s)\delta(\gamma-\gamma_s)\delta(\delta-\delta_s). \tag{B5}$$

To calculate P, equations (B3) and (B5) were substituted into equation (B1).

To calculate the estimation error in P associated with the fitting error in model $\boldsymbol{M}$, we analyzed the distribution of P_i using single realizations of the parameters to calculate $\rho_{\boldsymbol{M}}$, i.e., we substituted

$$\rho_{\boldsymbol{M},i} = \delta(\ln C_1-\ln C_{1,i})\delta(\alpha-\alpha_i)\delta(\beta-\beta_i)\delta(\gamma-\gamma_i)\delta(\delta-\delta_i) \tag{B6}$$

into equation (B1) to calculate a number of realizations of the probability P_i. The standard deviation of P_i is the estimation error.

C. STRENGTH OF THE GRAVITATIONAL WAVE BACKGROUND

In this section, we calculate the rms strength of the gravitational wave background in the residuals $\sigma_{\rm GW,2}(T)$ for a strain amplitude $h_c(f)$. The former quantity is the strength of the GW signal accessible to pulsar timing observations and is used to estimate the sensitivity of a PTA in §5.

The strain amplitude is usually modeled with power-law behavior over the range of f relevant to pulsar timing observations,

$$h_c(f) = A_0\left(\frac{f}{f_0}\right)^{\alpha}, \tag{C1}$$

and is characterized by an amplitude A_0 at frequency f_0.

The power spectrum $P_r(f)$ of the TOA fluctuations is related to the the strain amplitude $h_c(f)$ by (Hobbs et al. 2009a)

$$P_r(f) = \frac{h_c^2(f)}{12\pi^2 f^3}. \tag{C2}$$

The rms of the residuals $\sigma_{\rm GW,2}(T)$ over a time span T is related to the power spectrum of the perturbations $P_r(f)$ by

$$\sigma^2_{\rm GW,2}(T) = \int_0^\infty df H(f,T)P_r(f), \tag{C3}$$

where $H(f,T)$ is a high-pass filter that accounts for power that is removed by model fitting to the arrival times.

The rms of the residuals $\sigma_{\rm GW,2}$ is most accurately determined by simulating the TOA perturbations associated with a GWB and then calculating the residual TOAs and $\sigma_{\rm GW,2}$. For a gravitational wave background with $\alpha = -2/3$

$$\sigma_{\rm GW,2}(T) \approx 1.3\ {\rm ns}\ A_{0,-15}\left(\frac{T}{1\ {\rm yr}}\right)^{5/3}, \tag{C4}$$

where $A_{0,-15} = A_0/10^{-15}$ is the characteristic strain at $f_0 = 1\ {\rm yr}^{-1}$ and that the high pass filter is approximately unity for $f > 1/T$ and zero for $f < 1/T$. We note the scaling with T is similar to that for a random walk in frequency ($\rm RW_1$) for which $\sigma_{\rm TN,2} \propto T^{3/2}$ is expected.

The GWB was simulated using a large number of gravitational waves with wave amplitude, frequency, phase, polarization, and propagating direction randomly selected from appropriate PDFs. In particular, the wave amplitude

and frequency were selected from distributions consistent with Equation (C1) using appropriate lower f_ℓ and upper frequency cut-offs. Equation (C4) is valid for all $f_\ell \ll 1/T$. In simulations with $f_\ell = 1/(10T)$ we find that $\sigma_{\rm GW,2}(T) \approx 1/25\ \sigma_{\rm GW}(T)$.

REFERENCES

Arzoumanian, Z., Nice, D. J., Taylor, J. H., & Thorsett, S. E. 1994, ApJ, 422, 671
Bell, J. F., Bailes, M., Manchester, R. N., Lyne, A. G., Camilo, F., & Sandhu, J. S. 1997, MNRAS, 286, 463
Boynton, P. E., Groth, E. J., Hutchinson, D. P., Nanos, Jr., G. P., Partridge, R. B., & Wilkinson, D. T. 1972, ApJ, 175, 217
Camilo, F., et al. 2007, ApJ, 663, 497
Champion, D. J., et al. 2005, MNRAS, 363, 929
Cheng, K. S. 1987, ApJ, 321, 805
Chukwude, A. E. 2007, Chinese Journal of Astronomy and Astrophysics, 7, 521
Cordes, J. M., & Downs, G. S. 1985, ApJS, 59, 343
Cordes, J. M., & Helfand, D. J. 1980, ApJ, 239, 640
Cordes, J. M., & Shannon, R. M. 2008, ApJ, 682, 1152
Cordes, J. M., Wolszczan, A., Dewey, R. J., Blaskiewicz, M., & Stinebring, D. R. 1990, ApJ, 349, 245
D'Alessandro, F., McCulloch, P. M., Hamilton, P. A., & Deshpande, A. A. 1995, MNRAS, 277, 1033
D'Alessandro, F., McCulloch, P. M., King, E. A., Hamilton, P. A., & McConnell, D. 1993, MNRAS, 261, 883
Demorest, P. B. 2007, PhD thesis, University of California, Berkeley
—. 2008, http://www.nanograv.org/presentations/IPTA/PTA_Workshop_Demorest.pdf
den Hartog, P. R., Kuiper, L., Hermsen, W., Kaspi, V. M., Dib, R., Knödlseder, J., & Gavriil, F. P. 2008, A&A, 489, 245
Detweiler, S. 1979, ApJ, 234, 1100
Dewey, R. J., & Cordes, J. M. 1989, in Timing Neutron Stars, ed. H. Ögelman & E. P. J. van den Heuvel, 119
Dib, R., Kaspi, V. M., & Gavriil, F. P. 2008, ApJ, 673, 1044
Edwards, R. T., Hobbs, G. B., & Manchester, R. N. 2006, MNRAS, 372, 1549
Foster, R. S., Lyne, A. G., Shemar, S. L., & Backer, D. C. 1994, AJ, 108, 175
Gavriil, F. P., & Kaspi, V. M. 2002, ApJ, 567, 1067
Gotthelf, E. V., Gavriil, F. P., Kaspi, V. M., Vasisht, G., & Chakrabarty, D. 2002, ApJ, 564, L31
Harding, A. K., Shinbrot, T., & Cordes, J. M. 1990, ApJ, 353, 588
Helfand, D. J., Taylor, J. H., Backus, P. R., & Cordes, J. M. 1980, ApJ, 237, 206
Hellings, R. W., & Downs, G. S. 1983, ApJ, 265, L39
Hobbs, G., et al. 2009a, MNRAS, 394, 1945
Hobbs, G., Lyne, A. G., & Kramer, M. 2010, MNRAS, 402, 1027
Hobbs, G., Lyne, A. G., Kramer, M., Martin, C. E., & Jordan, C. 2004, MNRAS, 353, 1311
Hobbs, G. B., et al. 2009b, Publications of the Astronomical Society of Australia, 26, 103
Hotan, A. W., Bailes, M., & Ord, S. M. 2006, MNRAS, 369, 1502
Hurley, K., et al. 2005, Nature, 434, 1098
Jacoby, B. A., Bailes, M., van Kerkwijk, M. H., Ord, S., Hotan, A., Kulkarni, S. R., & Anderson, S. B. 2003, ApJ, 599, L99
Jaffe, A. H., & Backer, D. C. 2003, ApJ, 583, 616
Janssen, G. 2008, http://www.nanograv.org/presentations/IPTA/PTA_Workshop_Janssen_Verbeist.pdf
Jenet, F. A., Hobbs, G. B., Lee, K. J., & Manchester, R. N. 2005, ApJ, 625, L123
Jenet, F. A., et al. 2006, ApJ, 653, 1571
Jones, P. B. 1990, MNRAS, 246, 364
Kaplan, D. L., & van Kerkwijk, M. H. 2005, ApJ, 628, L45
Kaspi, V. M., Gavriil, F. P., Chakrabarty, D., Lackey, J. R., & Muno, M. P. 2001, ApJ, 558, 253
Kaspi, V. M., Taylor, J. H., & Ryba, M. F. 1994, ApJ, 428, 713
Konacki, M., & Wolszczan, A. 2003, ApJ, 591, L147
Kramer, M., Lyne, A. G., O'Brien, J. T., Jordan, C. A., & Lorimer, D. R. 2006, Science, 312, 549
Lange, C., Camilo, F., Wex, N., Kramer, M., Backer, D. C., Lyne, A. G., & Doroshenko, O. 2001, MNRAS, 326, 274
Lazaridis, K., et al. 2009, MNRAS, 400, 805
Lommen, A. N. 2002, PhD thesis, University of California, Berkeley
Lyne, A., Hobbs, G., Kramer, M., Stairs, I., & Stappers, B. 2010, Science, 329, 408
Manchester, R. N. 2008, http://www.nanograv.org/presentations/IPTA/PTA_Workshop_Manchester.ppt
Manchester, R. N. 2009, in IAU General Assembly
Manchester, R. N., Hobbs, G. B., Teoh, A., & Hobbs, M. 2005, AJ, 129, 1993
Matsakis, D. N., Taylor, J. H., & Eubanks, T. M. 1997, A&A, 326, 924
McLaughlin, M. A., et al. 2009, MNRAS, 400, 1431
Ord, S. M., Jacoby, B. A., Hotan, A. W., & Bailes, M. 2006, MNRAS, 371, 337
Sesana, A., & Vecchio, A. 2010, arXiv:1001.3161
Smits, R., Kramer, M., Stappers, B., Lorimer, D. R., Cordes, J., & Faulkner, A. 2009, A&A, 493, 1161
Splaver, E. M. 2004, PhD thesis, Princeton University
Thereau, G. 2008, http://www.nanograv.org/presentations/IPTA/PTA_Workshop_Theureau.pdf
Urama, J. O., Link, B., & Weisberg, J. M. 2006, MNRAS, 370, L76
van Haasteren, R., Levin, Y., McDonald, P., & Lu, T. 2009, MNRAS, 395, 1005
van Leeuwen, J., & Stappers, B. W. 2010, A&A, 509, A260000+
van Straten, W. 2006, ApJ, 642, 1004
Verbiest, J. P. W. 2009, PhD Thesis, Swinburne University, arXiv:0906.4246
Verbiest, J. P. W., et al. 2009, MNRAS, 400, 951
—. 2008, ApJ, 679, 675
Woods, P. M., et al. 2000, ApJ, 535, L55
You, X. P., et al. 2007, MNRAS, 378, 493
Zou, W. Z., Wang, N., Wang, H. X., Manchester, R. N., Wu, X. J., & Zhang, J. 2004, MNRAS, 354, 811

Table 5
Previous Timing Campaigns

Reference	Objects	$T_{\rm typ}$ (yr)	Observation Type
Canonical Pulsars (CPs)			
Helfand et al. (1980)	37	4	TW
Cordes & Downs (1985)	27	10	TN
D'Alessandro et al. (1993)	45	4	TW
Arzoumanian et al. (1994)	96	3	TW
Foster et al. (1994)	1	6	T*
D'Alessandro et al. (1995)	45	7	TN
Hobbs et al. (2004)	346, 27 MSP	20	TSW
Zou et al. (2004)	2	1	T
Champion et al. (2005)	15, 1 MSP	2	T
Kaplan & van Kerkwijk (2005)	1	11	T
Chukwude (2007)	27	10	S
McLaughlin et al. (2009)	6 RRAT	6	T
Hobbs et al. (2010)	346, 30 MSP	25	TSW
Millisecond Pulsars (MSPs)			
Kaspi et al. (1994)	2	2	S
Bell et al. (1997)	4	3	T
Lommen (2002)	4, 2 CP	10	S
Hotan et al. (2006)	15	2	S
Ord et al. (2006)	1	4	S
Demorest (2007)	15	2	T
Verbiest et al. (2008)	1	10	T
Hobbs et al. (2009b)	20	4	T
Lazaridis et al. (2009)	1	14	T
Verbiest (2009)	19	10	H
Magnetars (MAGs)			
Woods et al. (2000)	1	1	S
Kaspi et al. (2001)	4	1	S
Gavriil & Kaspi (2002)	5	1	S
Gotthelf et al. (2002)	1	2	S
Camilo et al. (2007)	1	1	S
den Hartog et al. (2008)	3	1	S
Dib et al. (2008)	1	1	S

Note. — Timing campaigns used in this analysis. We list campaigns, class of objects studied, typical observing length $T_{\rm typ}$, and reported observable. Horizontal lines divide campaigns that study predominantly canonical pulsars (CPs, $1/6\ {\rm s}^{-1} < \nu < 50\ {\rm s}^{-1}$), millisecond pulsars (MSPs; $\nu > 50\ {\rm s}^{-1}$), and magnetars (MAGs, $\nu < 1/6$ s). The rotating radio transients (RRATs) are rotating neutron stars that show spin properties similar to that of canonical pulsars. The reported observation types are: TW, total rms residuals and whitened residuals; TN, timing noise, S, higher order spindown terms (e.g., $\ddot{\nu}$), STW, spindown terms, total rms (after measurement of spin-down terms), and whitened residuals; H, harmonically related sinusoids and whitened residuals; T, only upper limits on levels of timing noise are reported; T*, only the total rms is reported but timing noise is dominant contribution to rms residuals.

Table 6
Timing Noise in PSR B1937+21

T (yr)	$\sigma_{\rm RMS}$ (μs)	$N_{\rm TOA}$	Ref.
1.0	0.15	···	1
1.0	0.23	22	2
1.0	0.24	19	2
1.0	0.32	16	2
1.0	0.24	16	2
1.0	0.21	18	2
1.0	0.21	14	2
1.0	0.19	23	2
1.2	0.21	13	2
1.5	0.17	···	3
2.0	0.25	47	2
2.0	0.29	38	2
2.0	0.20	38	2
2.2	0.20	38	2
2.3	0.19	···	4
2.4	0.20	231	5
2.7	0.32	85	6
4.0	0.20	39	7
4.0	0.30	···	8
4.0	0.41	85	2
4.2	0.49	80	2
4.4	0.27	168	9
8.2	0.94	440	2
10.0	1.3	···	10
16.8	9.3	387	10
20.0	112.0	400	11
23.3	24.2	588	12
24.0	27.4	···	13

Note. — Root mean square times of arrival for PSR B1937+21 for different observing programs. Column T shows the observing span, column $\sigma_{\rm RMS}$ shows the total rms residuals, column $N_{\rm TOA}$ shows the number of times of arrival included in the analysis, and column Ref. shows the numbered references. The references are: (1) Manchester (2008); (2) Kaspi et al. (1994); (3) Manchester (2009); (4) You et al. (2007); (5) Hotan et al. (2006); (6) Demorest (2007); (7) Demorest (2008); (8) Thereau (2008); (9) Verbiest (2009); (10) Lommen (2002); (11) Hobbs et al. (2004); (12) Verbiest et al. (2009); (13) Janssen (2008).

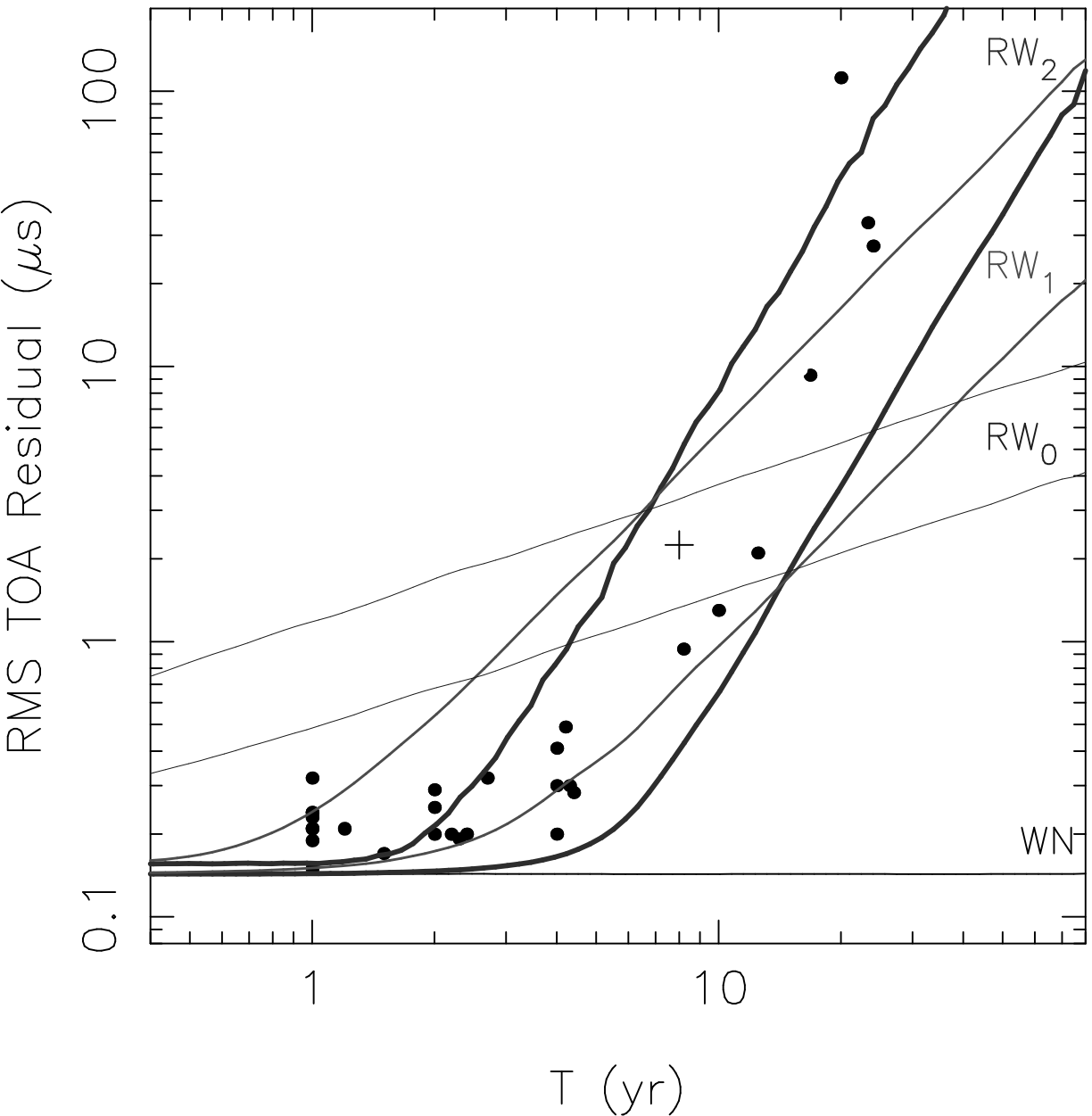
RMS TOA Residual (μs)
0.1
1
10
100
1
10
T (yr)
RW$_2$
RW$_1$
RW$_0$
WN